The Astrophysical Journal, 795:170 (11pp), 2014 November 10 doi:10.1088/0004-637X/795/2/170

THE SUPERNOVA PROGENITOR MASS DISTRIBUTIONS OF M31 AND M33: FURTHER EVIDENCE FOR AN UPPER MASS LIMIT

Zachary G. Jennings[1], Benjamin F. Williams[2], Jeremiah W. Murphy[4], Julianne J. Dalcanton[2], Karoline M. Gilbert[2,3], Andrew E. Dolphin[5], Daniel R. Weisz[1,2,6], and Morgan Fouesneau[2]
[1] University of California Observatories, Santa Cruz, CA 95064, USA; zgjennin@ucsc.edu
[2] Box 351580, The University of Washington Seattle, WA 98195, USA
[3] Space Telescope Science Institute, Baltimore, MD 21218, USA
[4] Department of Physics, Florida State University, Tallahassee, FL 32306, USA
[5] Raytheon, 1151 E. Hermans Road, Tucson, AZ 85706, USA; adolphin@raytheon.com
Received 2014 February 12; accepted 2014 September 23; published 2014 October 28

ABSTRACT

Using *Hubble Space Telescope* photometry to measure star formation histories, we age-date the stellar populations surrounding supernova remnants (SNRs) in M31 and M33. We then apply stellar evolution models to the ages to infer the corresponding masses for their supernova progenitor stars. We analyze 33 M33 SNR progenitors and 29 M31 SNR progenitors in this work. We then combine these measurements with 53 previously published M31 SNR progenitor measurements to bring our total number of progenitor mass estimates to 115. To quantify the mass distributions, we fit power laws of the form $dN/dM \propto M^{-\alpha}$. Our new larger sample of M31 progenitors follows a distribution with $\alpha = 4.4^{+0.4}_{-0.4}$, and the M33 sample follows a distribution with $\alpha = 3.8^{+0.4}_{-0.5}$. Thus both samples are consistent within the uncertainties, and the full sample across both galaxies gives $\alpha = 4.2^{+0.3}_{-0.3}$. Both the individual and full distributions display a paucity of massive stars when compared to a Salpeter initial mass function, which we would expect to observe if all massive stars exploded as SN that leave behind observable SNR. If we instead fix $\alpha = 2.35$ and treat the maximum mass as a free parameter, we find $M_{\rm max} \sim 35$–$45\ M_{\odot}$, indicative of a potential maximum cutoff mass for SN production. Our results suggest that either SNR surveys are biased against finding objects in the youngest (<10 Myr old) regions, or the highest mass stars do not produce SNe.

Key words: galaxies: individual (M31, M33) – supernovae: general

Online-only material: color figures

1. INTRODUCTION

While core-collapse supernovae (CCSNe) are linked both theoretically and observationally to the deaths of massive stars, the exact mapping between the mass of the progenitor and the nature of its death is an unresolved question. It is yet unknown exactly how the properties of a given star, specifically its mass, will affect the eventual SN type. Archival imaging of progenitor stars has been successful at linking Type II-P SNe to red supergiant (RSG) stars. However, it is difficult to predict the fate of more massive stars and the progenitors of uncommon SN types due to their rarity. Significant questions exist as to which mass ranges result in which types of SN, to what extent other properties such as metallicity affect this range, and whether all massive stars actually explode as SN.

Smartt et al. (2009) identified what they termed the "red supergiant problem"—an observed lack of progenitors between 18 and 30 $M_{\odot}$ which would be expected to explode as Type II SNe (see also Kochanek et al. 2008). They postulated that massive stars in this range may fail to explode as SNe, ending their lives in some other way. Horiuchi et al. (2011) compared measured massive star formation rates with the measured CCSN rate and found that twice as many massive stars are formed than explode as CCSNe. They explored a wide variety of explanations for this observation, and found that measurement errors on either rate could not solely explain the discrepancy. Smith et al. (2011a) examined observed rates of different SN types and found it impossible to explain the observed rates of more exotic SNe using solely single-star evolution. Kochanek (2014) explored the observed compact remnant mass function and found that it could be well-explained by a failed-SN scenario, where some massive stars did not actually produce SNe. Together, these recent studies all present evidence suggesting that a model in which all massive stars end their lives as SNe through single-star evolutionary channels is an incomplete picture.

Having a greater number of progenitor mass measurements naturally makes these issues easier to address. Unfortunately, direct imaging has requirements that limit the frequency with which it may be applied. Since one must directly observe the SN to identify the progenitor in pre-explosion imaging, one is clearly limited by the SN rate in the local universe. In addition, archival imaging of sufficient depth must exist, nearly always necessitating that the field in question has been previously imaged with either the Advanced Camera for Surveys (ACS), Wide-Field Planetary Camera 2 (WFPC-2), or Wide-Field Camera 3 (WFC3) instruments aboard the *Hubble Space Telescope* (*HST*). As a result of these limitations, only ~25 SN progenitors currently have mass constraints in the literature, and around half of these are only upper limits (Smartt et al. 2002; Van Dyk et al. 2003a, 2003b; Smartt et al. 2004; Maund et al. 2005; Hendry et al. 2006; Li et al. 2005, 2006, 2007; Smartt et al. 2009; Smartt 2009; Gal-Yam et al. 2007; Gal-Yam & Leonard 2009; Smith et al. 2011b; Maund et al. 2011; Van Dyk et al. 2011; Fraser et al. 2012; Van Dyk et al. 2012a, 2012b; Fraser et al. 2014; Maund et al. 2014a, 2014b).

In this work, we employ stellar population analysis as an alternative means of constraining the progenitor mass. The literature features many examples of using the age of a

[6] Hubble Fellow.

surrounding stellar population to constrain the progenitor stars of directly observed transients (Efremov 1991; Walborn et al. 1993; Panagia et al. 2000; Barth et al. 1996; Van Dyk et al. 1999; Maíz-Apellániz et al. 2004; Wang et al. 2005; Vinkó et al. 2009; Crockett et al. 2008; Gogarten et al. 2009a; Murphy et al. 2011). Stellar population analysis offers a means of constraining progenitor masses in cases where pre-explosion direct imaging does not exist, as well as a complementary constraint in cases where pre-explosion images of the progenitor are available.

Since one does not need to identify the specific progenitor star to determine the likely age of the star formation (SF) event that produced the progenitor, one may apply stellar population analysis to the locations of cataloged supernova remnants (SNRs), drastically increasing the number of potential progenitor measurements. While SNe are typically only visible on timescales of $\sim 10^2$ days, SNR remain observable for $\sim 10^4$ yr. Assuming an SNe rate of $\sim 10^{-2}\,\mathrm{yr}^{-1}$ galaxy^{-1} (Cappellaro et al. 1999), one would naively expect to be able to make $\sim$100 progenitor mass estimates per galaxy, provided they are close enough for resolved stellar population analysis. While this approach naturally prevents direct investigation of the SN type, it offers in exchange the leverage to investigate more potential targets.

Only a few studies have explored this application so far. Badenes et al. (2009) used the star formation maps of Harris & Zaritsky (2009) to estimate progenitor ages and masses for 8 SNR in the LMC. In Jennings et al. (2012, hereafter J12), we identified *HST*-observed fields coincident with cataloged SNR in M31 and analyzed resolved stellar photometry of the surrounding stellar population. We created color–magnitude diagrams (CMDs) of these populations and fit them to recover the star formation histories (SFHs). By identifying coeval populations in the SFH, we assigned likely ages and therefore likely masses to the SN progenitors. Our final result consisted of mass estimates for 53 likely CCSN progenitors, which we presented as a mass distribution. The primary finding in J12 was a paucity of massive stars in the recovered mass distribution when compared to a Salpeter initial mass function (IMF; Salpeter 1955). This suggests that some fraction of massive stars are not exploding as SNe which leave behind observable SNR, in agreement with the evidence found in the above studies.

This paper represents several extensions to the work presented in J12. First, we more than double the number of total progenitor star mass estimates, improving the statistics on our mass distribution fitting. We analyze 29 additional SNRs in M31 for which we have recently acquired new Panchromatic Hubble Andromeda Treasury (PHAT; Dalcanton et al. 2012) data. Second, we have expanded our sample to M33, an environment with roughly half the metallicity of M31 (Barker et al. 2011), by analyzing 33 additional M33 SNRs from various archival *HST* data sets. We also verify our result against potential biases due to host galaxy inclination or type. Finally, we update our mass distribution fitting method to a probabilistic framework, based on Markov Chain Monte Carlo (MCMC) techniques, in which we reliably include our mass uncertainties.

An outline of the paper is as follows: In Section 2 we briefly summarize our technique of mass estimation and discuss the SNR catalogs used in this study. In Section 3, we present our mass estimations for the additional regions measured in this study. In Section 4 we discuss the mass distributions of our SNR progenitors. Finally, in Section 5, we summarize the main conclusions of the paper.

2. METHODS

In this section, we provide a brief summary of the main points of our methodology; the full details of our technique are presented in J12.

2.1. Data Selection and Photometry

First, we select SNRs from catalogs which overlap with *HST* fields in M31 and M33. We limited our search to fields observed with the ACS and WFPC-2 instruments, as the optical CMDs tend to be deeper and offer the best SFH constraints. For M31, we combine three SNR catalogs to select targets from: Braun & Walterbos (1993); Magnier et al. (1995); Williams et al. (1995). All three catalogs make use of [S II]-to-Hα ratios to identify SNR. Our M33 SNR catalog comes from Long et al. (2010), who selected SNRs using both [S II]-to-Hα ratios and X-ray observations. Long et al. (2010) incorporated all previous SNR catalogs from the literature in their analysis. As mentioned in Section 1, all new M31 data analyzed in this work come from newly available PHAT data sets and therefore have uniform filters and exposure times, while the M33 data comes from various archival data sets coincident with SNR. The locations of SNRs analyzed in this paper and J12 are plotted in Figure 1. The full list of SNRs analyzed, including the associated *HST* data sets used, are in Table 1.

We used the photometry pipeline from the ACS Nearby Galaxy Treasury Program (Dalcanton et al. 2009) and the PHAT Program (Dalcanton et al. 2012) to perform resolved stellar photometry on all stars in the selected fields. The full details of how this photometry is performed are provided in Dalcanton et al. (2009, 2012). Briefly, the pipeline uses DOLPHOT (Dolphin 2000) to fit the well-characterized ACS point-spread function to all of the point sources in the image. Photometric measurements are then converted to Vega magnitudes using zero-points from the ACS handbook. We use fake star tests to assess photometric uncertainties and completeness; 10^5 fake stars of known color and magnitude are inserted into the full fields and blindly recovered using the identical software.

We assume distance moduli of 24.47 to M31 (McConnachie et al. 2005) and of 24.69 to M33 (Barker et al. 2011). Typical uncertainties of from these surveys are $\sim$0.05 mag for M31 and $\sim$0.1 mag for M33. We fix the distance moduli to these values for the remainder of the paper.

We found in J12 that it was difficult to constrain older SF events in shallow fields. We defined the "depth" of the field as the point at which photometric completeness dropped below 50% and adopted the same depth cut as J12 for this work. The values used are $F475W = 24.5$ for M31 data, shifted to $F475W = 24.7$ for the M33 fields. In practice, nearly all the fields examined in this work have depths significantly below these depth limits, making the precise placement of the cut largely unimportant.

2.2. SFH Measurement and Age Determination

After performing full-field photometry, we select all stars in an annulus of $\sim$50 pc around the location of the SNR of interest, which we use to then measure the SFH of the region. We use the software package MATCH (Dolphin 2002) to fit the observed CMD with synthetic ones based on the models of Marigo et al. (2008); Girardi et al. (2010). For purposes of populating the models, we assume a Salpeter IMF ($dN/dM \propto M^{-2.35}$) and a binary fraction of 0.35. J12 and Gogarten et al. (2009a) found no appreciable effect on measured SFH values from reasonable

Table 1
Sample SNRs for M31 and M33

SNR ID[a]	R.A. (J2000) (deg)	Dec. (J2000) (deg)	*HST* Field[b]	*HST* Program ID	Instrument	Filters & 50% Completeness Limits	Catalog[c]
			M31 SNRs				
2-038	10.9933	41.223	B02F04	12073	ACS/WFC	F475W = 27.06, F814W = 25.74	1
2-039	11.0173	41.2853	B04F10	12107	ACS/WFC	F475W = 27.23, F814W = 25.82	1
2-040	11.0228	41.3423	B04F05	12107	ACS/WFC	F475W = 27.21, F814W = 25.69	1
2-041	11.0285	41.2678	B04F10	12107	ACS/WFC	F475W = 27.11, F814W = 25.84	1
2-042	11.0463	41.2721	B04F10	12107	ACS/WFC	F475W = 27.47, F814W = 26.11	1
2-043	11.0848	41.3002	B04F04	12107	ACS/WFC	F475W = 27.43, F814W = 26.09	1
2-052	11.4151	41.7867	B14F04	12072	ACS/WFC	F475W = 27.39, F814W = 26.21	1
2-053	11.4313	41.8822	B16F05	12106	ACS/WFC	F475W = 27.67, F814W = 26.37	1
2-054	11.4661	41.7114	B14F15	12072	ACS/WFC	F475W = 27.56, F814W = 26.24	1
BW45	10.8796	41.1996	B02F11	12073	ACS/WFC	F475W = 26.78, F814W = 25.33	2
BW51	10.9729	41.2011	B02F04	12073	ACS/WFC	F475W = 27.23, F814W = 25.96	2
BW58	11.0562	41.3319	B04F04	12107	ACS/WFC	F475W = 27.42, F814W = 25.92	2
BW59	11.0775	41.3146	B04F04	12107	ACS/WFC	F475W = 27.46, F814W = 25.98	2
BW63	11.1321	41.3933	B06F10	12105	ACS/WFC	F475W = 27.44, F814W = 26.1	2
BW64	11.1325	41.3986	B06F10	12105	ACS/WFC	F475W = 27.44, F814W = 26.1	2
BW79	11.2542	41.4734	B08F03	12075	ACS/WFC	F475W = 27.29, F814W = 26.11	2
BW94	11.4029	41.8997	B16F05	12106	ACS/WFC	F475W = 27.52, F814W = 26.42	2
BW95	11.4083	41.8955	B16F05	12106	ACS/WFC	F475W = 27.54, F814W = 26.42	2
BW96	11.4104	41.7999	B14F04	12072	ACS/WFC	F475W = 27.29, F814W = 26.18	2
BW98	11.4154	41.7316	B14F10	12072	ACS/WFC	F475W = 27.43, F814W = 26.04	2
BW100	11.435	41.7648	B14F10	12072	ACS/WFC	F475W = 27.75, F814W = 26.46	2
BW101	11.4354	41.7331	B14F09	12072	ACS/WFC	F475W = 27.62, F814W = 26.39	2
K293	11.0277	41.3325	B04F05	12107	ACS/WFC	F475W = 27.1, F814W = 25.68	3
K413	11.1076	41.4136	B06F04	12105	ACS/WFC	F475W = 27.25, F814W = 25.82	3
K638	11.2495	41.4728	B08F03	12075	ACS/WFC	F475W = 27.37, F814W = 26.11	3
K763	11.3537	41.7284	B14F17	12072	ACS/WFC	F475W = 27.35, F814W = 25.96	3
K774	11.3607	41.7147	B12F05	12071	ACS/WFC	F475W = 27.54, F814W = 26.2	3
K782	11.3653	41.7175	B12F05	12071	ACS/WFC	F475W = 27.54, F814W = 26.2	3
K817	11.3973	41.7863	B14F04	12072	ACS/WFC	F475W = 27.42, F814W = 26.11	3
K854A	11.4375	41.9152	B16F05	12106	ACS/WFC	F475W = 27.65, F814W = 26.34	3
			M33 SNRs				
20	23.2874	30.4497	ANY	10190	ACS/WFC	F606W = 27.14, F814W = 26.49	4
30	23.3402	30.5253	ANY	10190	ACS/WFC	F606W = 27.03, F814W = 26.31	4
34	23.367	30.5264	ANY	10190	ACS/WFC	F606W = 26.71, F814W = 26.12	4
37	23.3727	30.8197	H10	5914	WFPC2	F555W = 26.73, F814W = 25.67	4
38	23.3759	30.7955	H10	5914	WFPC2	F555W = 26.5, F814W = 25.36	4
40	23.3806	30.7051	ANY	9873	WFPC2	F606W = 25.36, F814W = 25.31	4
41	23.3825	30.517	ANY	10190	ACS/WFC	F606W = 26.76, F814W = 26.18	4
43	23.3975	30.7089	ANY	9873	WFPC2	F606W = 25.69, F814W = 24.67	4
44	23.3984	30.8231	H10	5914	WFPC2	F555W = 27.03, F814W = 25.84	4
48	23.4084	30.7051	ANY	9873	WFPC2	F606W = 26.14, F814W = 24.89	4
49	23.4194	30.6613	ANY	10190	ACS/WFC	F606W = 25.52, F814W = 24.77	4
50	23.4197	30.7099	ANY	9873	WFPC2	F606W = 25.13, F814W = 24.09	4
57	23.4321	30.6032	DISK1	10190	ACS/WFC	F475W = 26.93, F814W = 25.75	4
58	23.4386	30.5389	SRV6	6640	WFPC2	F555W = 25.59, F814W = 24.44	4
59	23.4477	30.6624	ANY	10190	ACS/WFC	F606W = 24.89, F814W = 24.52	4
61	23.4521	30.5522	SRV6	6640	WFPC2	F555W = 25.48, F814W = 24.29	4
62	23.4573	30.5138	SRV6	6640	WFPC2	F555W = 25.91, F814W = 24.75	4
63	23.4579	30.5046	H38	5914	WFPC2	F555W = 26.1, F814W = 24.89	4
64	23.4588	30.5913	DISK1	10190	ACS/WFC	F475W = 26.86, F814W = 25.71	4
66	23.4653	30.5166	SRV6	6640	WFPC2	F555W = 25.93, F814W = 24.77	4
67	23.4655	30.5121	SRV7	6640	WFPC2	F555W = 26.27, F814W = 25.06	4
69	23.4762	30.5633	ANY	10190	ACS/WFC	F606W = 25.61, F814W = 24.52	4
71	23.4788	30.5531	ANY	10190	ACS/WFC	F606W = 25.78, F814W = 25.01	4
74	23.4874	30.583	DISK1	10190	ACS/WFC	F475W = 26.85, F814W = 25.75	4
75	23.488	30.6801	R14	5914	WFPC2	F555W = 24.77, F814W = 23.53	4
76	23.488	30.585	DISK1	10190	ACS/WFC	F475W = 26.82, F814W = 25.75	4
77	23.4919	30.536	ANY	10190	ACS/WFC	F606W = 26.06, F814W = 25.4	4
80	23.4934	30.6068	DISK1	10190	ACS/WFC	F475W = 26.81, F814W = 25.69	4
81	23.4938	30.559	ANY	10190	ACS/WFC	F606W = 25.38, F814W = 24.99	4
83	23.4997	30.5726	ANY	10190	ACS/WFC	F606W = 25.61, F814W = 24.78	4

Table 1
(Continued)

SNR ID [a]	R.A. (J2000) (deg)	Dec. (J2000) (deg)	*HST* Field [b]	*HST* Program ID	Instrument	Filters & 50% Completeness Limits	Catalog [c]
			M33 SNRs				
84	23.5013	30.7054	R14	5914	WFPC2	F555W = 24.96, F814W = 23.78	4
91	23.5177	30.5492	ANY	10190	ACS/WFC	F606W = 25.88, F814W = 25.03	4
134	23.7352	30.6064	ANY	9873	WFPC2	F606W = 27.61, F814W = 26.46	4

Notes.
[a] IDs taken from respective catalogs.
[b] Field designation as listed in MAST.
[c] Catalogs 1, 2, 3, and 4 are Magnier et al. (1995), Williams et al. (1995), Braun & Walterbos (1993), and Long et al. (2010) respectively.

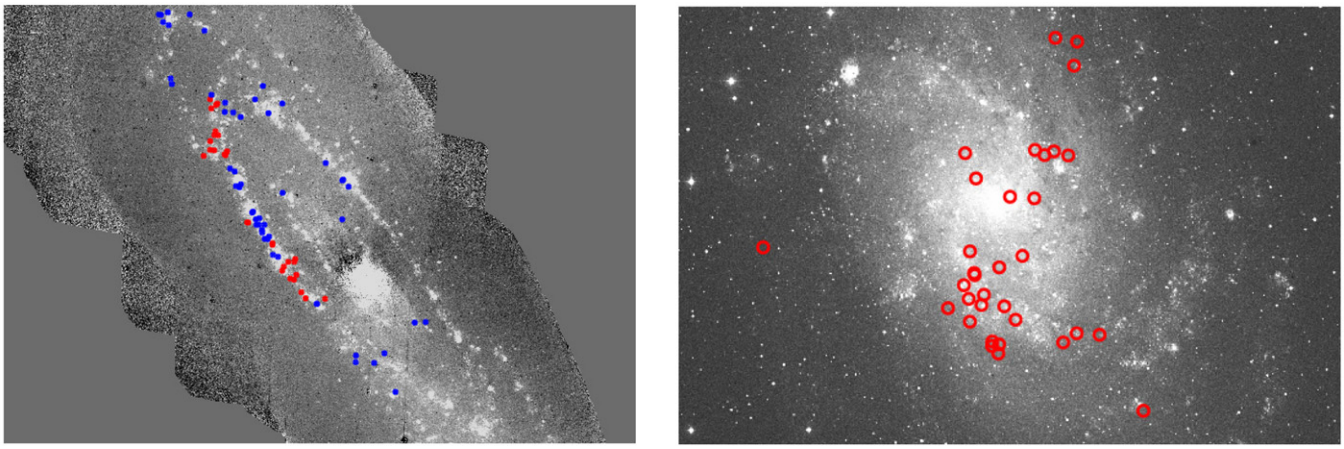

Figure 1. Left panel: locations of the combined M31 SNR sample superposed on a star-subtracted Hα image of M31 from Williams et al. (1995). SNRs from J12 are plotted in blue, while those from this paper are plotted in red. As the new M31 SNRs all come from recently acquired PHAT survey data, they are highly correlated spatially. Right panel: locations of M33 SNRs analyzed in this paper on a DSS image of M33.
(A color version of this figure is available in the online journal.)

variations of these parameters. MATCH also makes use of fake stars to evaluate completeness and photometric uncertainties, which we extract from an annulus ~2.5 times the size to ensure a sufficient number of fake stars. The distance modulus is fixed to the respective value for each galaxy from above. The CMD is binned with bin sizes 0.3 in magnitude and 0.15 in color. Metallicity is constrained to have a spread of ~0.15 dex, and to increase or stay constant with time.

Our age bins for SFH determination are in log-space from log(Age) = 6.60 (4 Myr) to log(Age) = 10.10 (12.5 Gyr) in steps of 0.05 dex. For a solar metallicity system, these ages would correspond to supernova progenitors of roughly 52 $M_{\odot}$ and 7.3 $M_{\odot}$ respectively. Note that any SF MATCH finds for ages younger than 4 Myr is included in the 4 Myr to 4.4 Myr bin. Thus SF found in this youngest bin actually acts as an upper limit on the age, constraining the SF to be younger than 4.4 Myr. The final result from our CMD fitting analysis is an SFH from the present back to 12.5 Gyr.

Our treatment of reddening in our CMD fitting was the same as in J12, and merits further discussion. Our prescription for reddening is to assume that A_V follows a top-hat distribution, the width of which is specified by a dA_V parameter defined by the user. MATCH then fits for the minimum value of this A_V distribution, defining the top-hat in the course of the fitting procedure. To determine the value of the parameter most appropriate for each SNR location, we increased the width of the dA_V parameter until the fit returned a reddening value consistent with the Schlegel et al. (1998) foreground reddening value. In other words, we treat all reddening in addition to foreground MW extinction as broadening of the CMD due to differential reddening.

2.3. Age/Mass Conversion

For purposes of age/mass conversion, we use the same models as those fitted to the CMDs. For each age bin, we assume the star with the largest zero-age main sequence mass ($M_{\rm ZAMS}$) remaining in the isochrone will be the next one to become a SN. This mass is then taken as the progenitor mass for that given age bin. We perform a simple linear interpolation across age bins to get an estimated progenitor mass for an arbitrary age. We adopt the $Z = 0.019$ isochrones for M31 and the $Z = 0.008$ isochrones for M33, which are consistent with gas-phase metallicity measurements for the two galaxies (Blair et al. 1982; Barker et al. 2011). However, as demonstrated in J12, the choice of metallicity is largely unimportant in converting age to mass as the $M_{\rm ZAMS}$ masses are very similar across reasonable ranges of metallicity. For a given age, the difference in mass between the two isochrones is typically a few percent.

Numerous sources of theoretical and observational evidence point toward a minimum mass necessary for a star to undergo core collapse. We wish to identify the age range where a population may still produce an SN. Coeval populations that are too old will have no stars remaining massive enough to become core-collapse SNe. In J12, we found our data most consistent with a minimum mass of 7.3 $M_{\odot}$, corresponding to an age of

50 Myr. We verified that our new data are also consistent with this minimum mass, and therefore only consider ages $\leqslant$50 Myr in our age distributions. However, we were not able to improve this constraint using our current data set.

We do not assume any maximum mass at this stage. However, for ages younger than 4.4 Myr, we may only quote a limit on the progenitor mass of $>52\,M_{\odot}$ for the $Z = 0.019$ isochrone (i.e., M31) and $>55\,M_{\odot}$ for the $Z = 0.008$ isochrone (i.e., M33) because the optical CMDs are degenerate for ages younger than 4.4 Myr.

To estimate the age of the progenitor, we identify the age at which, over the past 50 Myr, 50% of the stars have formed. This median age is then converted to a median mass using the interpolation defined above. We also assign uncertainties to the age from two sources using the methods discussed in the next section. Furthermore, we calculate full probability distributions for each progenitor. We assume that the progenitor originates from any SF that has occurred in the region over the past 50 Myr, where the fraction of stellar mass formed in a given age bin corresponds to the probability that the progenitor star was of that age. Thus, all of our probability distributions sum to one because they include all SF that has occurred over the past 50 Myr.

2.4. Treatment of Uncertainties

Uncertainties on the age estimate may arise either from uncertainties in the CMD fitting process, or from the age spread present in the stellar population.

To characterize uncertainties from fitting, we use a Monte Carlo (MC) technique in which we resample the CMD to account for Poisson noise using the MATCH software (see Dolphin 2002). We also apply random shifts to the isochrones in temperature, with $\sigma = 0.02$, and bolometric luminosity, with $\sigma = 0.17$, during this procedure. These random shifts are intended to mimic potential uncertainties in the stellar evolution models themselves. The magnitude of the luminosity shift is also larger than the uncertainty in the distance, thereby incorporating those uncertainties. Each resampling is then refit using our identical CMD fitting procedure, but with fixed reddening. These resulting SFHs provide uncertainties on the SF in a given bin. With these uncertainties, we calculate a probability distribution for the value of the median age. We adopt the 16% and 84% range of this distribution as our uncertainty in the median age.

Another source of uncertainty is the intrinsic spread of the SFH across multiple age bins. There are many SNR populations in which there are two (or more) distinct SF events, and certainly some where a single SF event may spread across two or more adjacent bins. To account for this, we find the locations where 16% and 84% of the stellar mass was formed and adopt these as our uncertainties due to the spread of SF. These age-spread uncertainties therefore include an age range that contains 68% of the young stellar mass present in the region.

We add these two sources of uncertainty in quadrature to find our final (potentially asymmetric) estimates of uncertainty on the median age. Finally, we argue that we cannot truly constrain our progenitors to any better precision that that afforded by the age bins in which we have performed our CMD fitting. In other words, we always round our uncertainties to the nearest age bin boundary.

In practice, the second source of uncertainty due to the spread of SF across multiple age bins tends to dominate that provided by the random uncertainties in the fitting process. This is because, while the fitting process may affect the amount of SF found in a given bin, the change in SF must be very large to modify the estimate of the *median* age. The random uncertainty must be enough to significantly change the relative prominence of a preferred burst of SF. For most of the MC realizations, it is not, and as a result, the spread of SF tends to be the largest factor.

The final source of uncertainty, which we neglect in determining our final answers, is the conversion from age to mass, which depends on the models applied. We do not include this uncertainty in our mass tables, as our uncertainties assume the Marigo et al. (2008) and Girardi et al. (2010) models to be consistent with our SFH fitting as they are used in both processes. In J12, we estimated that the effects of applying different models for the age/mass conversion would potentially be $\sim$0.5–1.0 $M_{\odot}$ (younger ages have larger uncertainty) by comparing the predicted masses of Pietrinferni et al. (2004) with those of Marigo et al. (2008) and Girardi et al. (2010). However, as we have used the Marigo et al. (2008) and Girardi et al. (2010) models to derive these ages in the first place, it is not clear that comparing the Pietrinferni et al. (2004) masses to those of our chosen isochrones is reflective of the actual data.

2.5. Assumptions in our Methodology

We make multiple assumptions in our technique based upon justifications detailed in J12. In this section, we briefly review these assumptions and their potential impacts on our conclusions.

First, naturally, in using the surrounding stellar population to infer information about the progenitor star, we are assuming that the two are evolutionarily linked. Given that the vast majority of stars form in clusters (Lada & Lada 2003) with coeval populations, and that that these populations remain spatially associated on 50 pc scales for 50 Myr, we expect this to be a reasonable assumption (see also Bastian & Goodwin 2006; Gogarten et al. 2009b; Eldridge et al. 2011).

Related to this point is that our methodology is also contingent on the accuracy, completeness, and selection effects of the SNR catalogs used. If the SNR catalogs are biased toward one specific type of progenitor or environment, this could bias the overall inferred distribution. Braun & Walterbos (1993) and Magnier et al. (1995) both consider extinction to be a minor problem. Both studies note that detection biases may exist as a function of the age of the *remnant*, but do not note any biases toward any particular age of the surrounding stellar population. Related to this, we have also assumed that SNRs behave similarly in different environments. If SNRs in differently aged populations had significantly different lifetimes or luminosities, we would naturally be subject to selection effects from this.

We assume for our study that the SNR catalogs used are not biased toward any particular progenitor age, and we have included as many SNR locations as possible in our analysis. We note the consistency of the M33 and M31 results and the consistency between different subsets of the M31 sample, which depend on different SNR catalogs. This suggests that there are no significant selection biases imposed by the detection method or survey location. However, we have no real way to test the second caveat, that SNRs from differently aged populations have different lifetimes or detectability thresholds. We discuss this more in Section 4.3.

Next, our method provides no information about the type of SN which created the SNR. For CCSNe, this ambiguity does not affect the mass estimation process, since all CCSNe are linked to the deaths of massive stars and therefore young stellar

populations (although the mass distribution of progenitors as a function of SN type is certainly an interesting question, we are unable to investigate this with our methodology). We note that there could be contaminants from thermonuclear Type Ia SNe. However, Type Ia SNe will generally be associated with older stellar populations. The absence of any recent SF from the CMD analysis will allow one to remove some fraction of these contaminants. We identified six such SNRs with zero recent SF in J12. In this work, we only find one such SNR in our new M31 sample (K413) and zero such SNRs in our M33 sample. The new M31 data analyzed in this work essentially all comes from the star-forming ring of M31 due to the distribution of the PHAT survey, so it is not entirely surprising that nearly all fields analyzed return significant recent SF and that nearly all of the SNe are CCSNe. The result of all analyzed M33 SNR populations having young SF is also likely due to the fact that M33 has a higher SF intensity than M31.

Typical fractions of Type Ia SNe compared to all SNe are ~25%, although such a figure is dependent on the galaxy type in question (Li et al. 2011). We would expect a higher fraction for M31 and a lower fraction for M33 based on morphological distinction. In addition, there are many reasons to assume that this Ia fraction may actually be an upper limit, with a bias resulting from the faintness of type CCSNe compared to Type Ia SNe (see discussions in Thompson et al. 2009; Horiuchi et al. 2009; Horiuchi et al. 2011). Finally, both Braun & Walterbos (1993) and Magnier et al. (1995) explicitly note that they will be significantly more biased toward identifying CCSNe remnants over Type Ia remnants due to the spatial distribution of their surveys. We do not include the M31 bulge in our sample, where most of the Ia events would be expected to occur. Thus we actually expect Ia SNe in our sample to be a significantly smaller fraction than would be expected based on galaxy-wide SN rate studies.

Furthermore, in J12, we demonstrated that our results are robust to inclusion of additional misidentified Type Ia SNe by removing additional potential contaminants even up to 25%. We identified those SNR locations with minimal *GALEX* FUV flux and removed those objects from our sample. The resulting progenitor mass distribution was essentially unchanged (the 95% confidence interval on the power-law exponent changed from $2.7 < \alpha < 4.4$ to $2.6 < \alpha < 4.3$). We conclude that, while there is uncertainty associated with an individual progenitor mass measurement due to the possibility of it being a Type Ia SNe, the overall distributions of progenitor masses are largely robust to the inclusion of a few progenitors with random ages since the vast majority of our SNR will be the result of CCSNe. In other words, while there are almost certainly some Type Ia contaminants masquerading as CCSNe in our sample, they will be a small number and will not significantly modify the overall conclusions.

Finally, our method is contingent on the accuracy of the stellar evolution models used to populate our model CMDs. Our CMD-derived SFHs include estimates of these model uncertainties (see Section 2.4), although we neglect them during our mass conversion procedure. It is worth noting that studies of directly identified progenitor stars suffer from similar uncertainties in that they must fit the spectral energy distributions to derive a luminosity and temperature and use stellar evolution models to infer the mass of late-stage massive stars (e.g., Smartt et al. 2009). These are thought to be the most uncertain stages of the model predictions. Our approach makes use of the entire CMD, making our results less sensitive to the details of the late-stage stellar evolution models.

3. RESULTS

Examples of the process for mass determinations of M31 SNRs can be seen in J12. Two examples of the fitting process applied to M33 SNRs, 20 and 34, are displayed in Figures 2 and 3. The left panel of each plots the observed CMD in red points, with the best-fit model produced by MATCH in grayscale in the background. The right panel of both displays the cumulative fractional SFH over the past 50 Myr for each SNR, as fit by MATCH. The green highlighted region represents the 68% confidence interval for the age and mass estimates. The mass value is taken from where the cumulative line crosses the 50% cumulative fraction (marked with a blue line), with the upper and lower values given by the 68% confidence interval.

We provide these estimates for the M31 SNR in Table 2 and the M33 SNR in Table 3. We also include the number of main sequence stars and the total number of stars in the 50 pc region around the remnant, the total stellar mass formed over the past 50 Myr, and the dA_V parameter applied when fitting the CMDs.

The uncertainties on our age and mass measurements are calculated as described in Section 2.4. Note that for progenitors with a very precise age (e.g., 2-038), the quoted uncertainties are underestimated as our age-to-mass conversion uncertainty likely dominates. However, as it is not clear how to quantify this uncertainty, we do not include it in our quoted range. Progenitors with upper errors of "INDEF" have upper errors which exceed the mass range over which we can measure ($>52\,M_\odot$ for M31 and $>55\,M_\odot$ for M33). As a result, we may only apply lower limits for the masses of these progenitors. Indeed, three progenitors have *median* masses above our upper limit. We include these values for completeness in the table, but in truth the median mass is not meaningful in this case, at least in terms of assigning a mass to the progenitor star.

We present the collective progenitor mass distribution in two ways. Figure 4 shows a simple histogram of median progenitor masses. We plot histograms for the separate M31 and M33 distributions, as well as the combined sample of all progenitors. We include the histograms which would be expected to be observed if the SNe progenitor distribution followed a Salpeter IMF, with the total number of stars normalized to be the same as that included in the specified sample.

The right panel of Figure 4 displays the cumulative median mass distributions for the above samples. In addition, we also plot 100 randomly selected slopes from the MCMC fitting procedure (see Section 4.1), showing the approximate extent of the probability distribution for the mass function exponent. The highlighted orange line is for $\alpha = 4$. Note the apparent offset between the MCMC realizations of the function and the median progenitor distributions. This is due to the fact that many of the more massive progenitors have uncertainties extending back to significantly older ages, emphasizing the importance of properly considering the uncertainties in the mass estimates.

We also include, for reference, two Salpeter IMFs ($dN/dM \propto M^{-2.35}$), one integrated to 120 $M_\odot$ and one integrated to 35 $M_\odot$. Note that the measured distributions are all visibly steeper (featuring fewer high mass progenitors) than would be expected from a Salpeter IMF.

4. QUANTIFYING THE PROGENITOR MASS DISTRIBUTIONS

In this section, we present our analysis of the recovered progenitor mass distributions. We evaluate these distributions in two different ways. First, for comparison with J12, we apply the

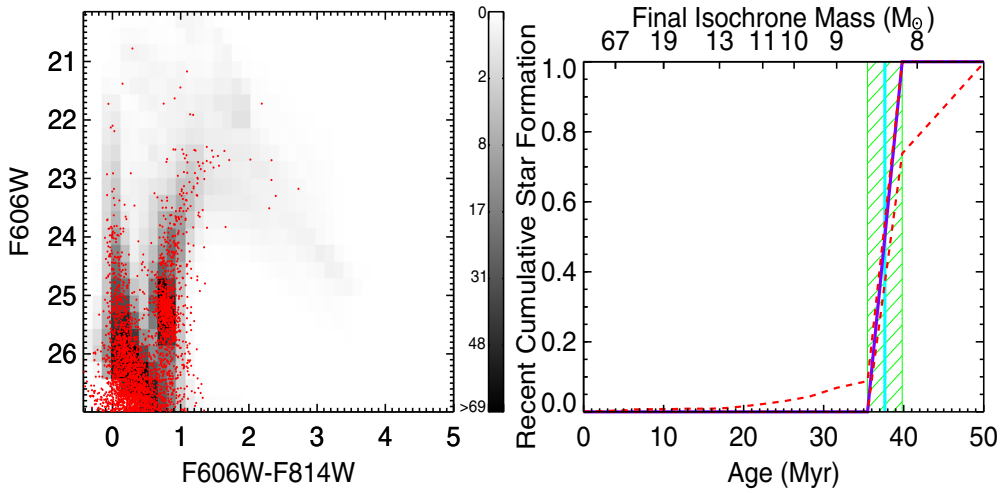

Figure 2. Left panel: red points are observed the F606W/F814W CMD for SNR 20 in M33. The background grayscale represents the best-fit model from MATCH, with the stellar density scale on the right. Right panel: cumulative fractional SFH from the best-fit MATCH model over the most recent 50 Myr. The best fit SFH is the purple line. The orange lines are 68% uncertainties. The cross-hatched green region represents the favored age and mass for this SNR progenitor, with uncertainties calculated as described in Section 2.4. The population features one prominent burst of SF, favoring a well-constrained mass of $8.6^{+0.3}_{-0.3}\ M_{\odot}$. The blue line represents the median age.

(A color version of this figure is available in the online journal.)

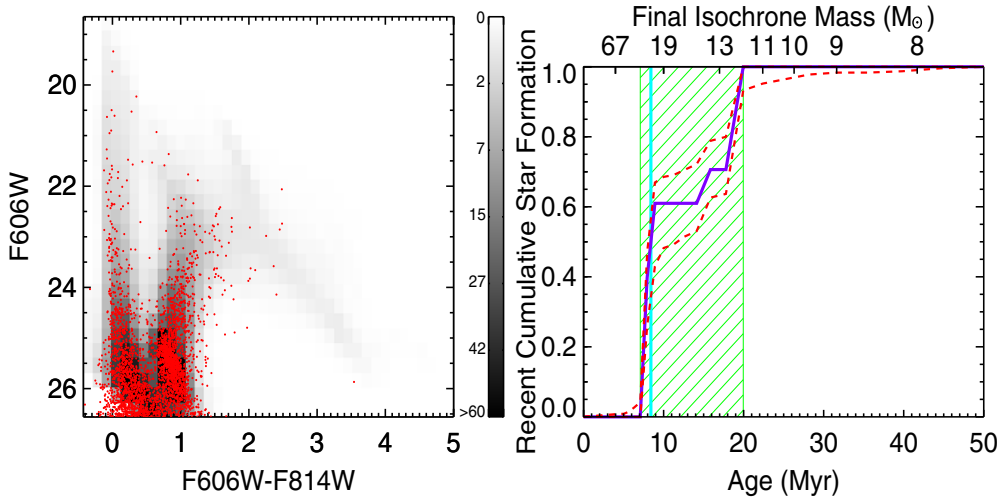

Figure 3. Left panel: red points are the observed F606W/F814W CMD for SNR 34 in M33. The background grayscale represents the best-fit model from MATCH, with the stellar density scale on the right. Right panel: cumulative fractional SFH from the best-fit MATCH model over the most recent 50 Myr. The best fit SFH is the purple line. The orange lines are 68% uncertainties. The cross-hatched green region represents the favored age and mass for this SNR progenitor, with uncertainties calculated as described in Section 2.4. The SFH is more spread out than in the example in Figure 2, favoring a mass of 24^{+4}_{-12}. The blue line represents the median age.

(A color version of this figure is available in the online journal.)

Kolmogorov–Smirnov (K-S) test between our distributions and those of several power law functions. Note that our use of the K-S test neglects uncertainties on our individual measurements, so we include it purely to verify the consistency of our current results with our previous analysis. Next, for reliable comparisons to models which properly include our uncertainties, we use a more sophisticated maximum-likelihood technique (adapted from Weisz et al. 2013) to fit power laws to our progenitor mass distributions. We use these maximum-likelihood inferred results for all scientific interpretations.

We first use a K-S test to verify the consistency of our results with J12. Our procedure is to take the observed distribution of the median masses for the listed segment of our sample and perform a one-sided K-S comparison to a sample IMF, defined as $dN/dM \propto M^{-\alpha}$. Values of α for which the K-S test returns a <5% chance ($P < 0.05$) of being from the same distribution are defined as being inconsistent with the given mass distribution at 95% confidence. For all IMF comparisons, we integrate the model IMF from 7.3 $M_{\odot}$, the minimum mass value we found in J12, to 120 $M_{\odot}$. The exact selection of the maximum mass value does not make a significant difference because very massive stars contributed little to the expected numbers.

The primary result from this analysis is that all of our sample selections (only M31, only M33, and combined) are inconsistent with a Salpeter IMF. The range of power-law indexes that are consistent with our simple median mass distributions according to the K-S test ($P > 0.05$) are 2.4–4.6 for M33, 3.8–4.8 for M31, and 3.7–4.3 for the combined sample. In other words, we have a paucity of massive stars in our progenitor distributions. We would expect to recover more massive stars if they have been formed following a Salpeter IMF and all explode as SNe. This finding is consistent with the main result of J12 by expansion to

Table 2
Progenitor Mass Results for Newly Analyzed M31 SNR Sample

SNR ID	M_{ZAMS} ($M_\odot$)	Progenitor Age (Myr)	MS Stars	Total Stars	Stellar Mass Formed (10^2 $M_\odot$)	Additional dA_V Applied (Total $dA_V - 0.5$)
			M31 SNR Progenitors			
2-038	$8.4^{+0.2}_{-0.2}$	38^{+2}_{-2}	191	4601	11	0.5
2-039	$7.6^{+1.4}_{-0.3}$	46^{+4}_{-14}	265	3940	25	0.5
2-040	$7.5^{+0.2}_{-0.2}$	47^{+3}_{-3}	272	5812	11	0.3
2-041	$8.4^{+8.8}_{-0.2}$	37^{+2}_{-26}	218	3666	31	0.7
2-042	17^{+1}_{-11}	11^{+52}_{-1}	187	4794	7	0.5
2-043	$8.1^{+0.4}_{-0.8}$	40^{+10}_{-4}	154	2177	12	0.3
2-052	$8.8^{+0.2}_{-0.3}$	33^{+2}_{-2}	272	4091	47	0.6
2-053	$7.9^{+0.2}_{-0.2}$	42^{+2}_{-2}	298	4126	22	0.8
2-054	$118^{+\mathrm{INDEF}}_{-110}$	$2.2^{+37.6}_{-1.5}$	343	3950	1	0
BW45	$8.5^{+17.5}_{-0.4}$	36^{+4}_{-29}	265	5434	81	0.6
BW51	$7.9^{+0.2}_{-0.2}$	42^{+2}_{-2}	207	4206	11	0.5
BW58	$8.6^{+8.6}_{-0.4}$	36^{+4}_{-24}	264	4993	18	0.3
BW59	$8.6^{+0.5}_{-0.9}$	35^{+9}_{-4}	298	4624	56	0.7
BW63	15^{+28}_{-6}	14^{+26}_{-9}	335	5009	38	0.1
BW64	13^{+4}_{-2}	16^{+6}_{-5}	384	5089	46	0.1
BW79	$7.6^{+4}_{-0.3}$	46^{+4}_{-26}	332	4611	9	0.3
BW94	$8.4^{+0.6}_{-0.3}$	37^{+3}_{-6}	326	4343	53	0.7
BW95	$8^{+9.1}_{-0.3}$	41^{+3}_{-30}	390	4568	42	0.6
BW96	$7.9^{+2.4}_{-0.5}$	43^{+7}_{-18}	451	3709	47	0.1
BW98	14^{+3}_{-4}	15^{+13}_{-4}	204	4239	11	0.4
BW100	$8.4^{+0.2}_{-0.2}$	38^{+2}_{-2}	332	4940	8	0.3
BW101	$8.2^{+0.4}_{-0.4}$	40^{+5}_{-4}	271	4822	40	0.4
K293	$8.8^{+\mathrm{INDEF}}_{-0.7}$	34^{+6}_{-31}	525	5682	47	0.4
K638	$7.9^{+0.2}_{-0.2}$	42^{+2}_{-2}	316	4749	7	0.3
K763	$9.2^{+0.5}_{-1.8}$	31^{+19}_{-3}	288	3650	16	0.2
K774	$8.4^{+0.2}_{-0.2}$	38^{+2}_{-2}	270	4694	8	0.1
K782	$7.9^{+0.2}_{-0.2}$	42^{+2}_{-2}	294	4616	17	0.3
K817	$8^{+5.4}_{-0.3}$	41^{+3}_{-26}	698	5068	38	0.3
K854A	14^{+1}_{-6}	16^{+34}_{-1}	366	4194	18	0.6
K413[a]	–	–	338	5364	0	0.1

Note. [a] K413 features no recent star formation. We interpret it as a likely Ia candidate and remove it from our combined mass distributions in subsequent analysis.

a larger sample, and supports a growing number of other lines of evidence suggesting that not all massive stars explode as SNe. However, because these comparisons do not take into account the uncertainties of our mass estimates, they do not represent a reliable characterization of the range of acceptable power-law indexes. Therefore, while it is encouraging to find consistency between J12 and our new larger samples, we now turn to more sophisticated fitting techniques to determine how well we can characterize the distributions with our current measurements.

4.1. MCMC Mass Distribution Fitting

To properly include uncertainties in our mass distribution fitting, we adopted a probabilistic framework developed by Weisz et al. (2013) to fit a power-law function to our mass distributions. A full probability distribution for the entire sample is created from the individual mass measurements and uncertainties. We then fit a power-law distribution using the Markov Chain Monte Carlo (MCMC) sampler *emcee* (Foreman-Mackey et al. 2013) to sample the posterior distributions. We then extracted the functional parameters and robust uncertainties from these posterior distributions. Quoted uncertainties correspond to the 16th and 84th percentiles of the probability distributions. When performing our fitting, we set a prior that $M_{max} > 20\ M_\odot$, and fixed the minimum mass to 7.3 $M_\odot$. As an illustration of the distribution of power-law indices, we plot 100 randomly selected MCMC steps in Figure 4.

We found that we were unable to constrain the maximum mass beyond our prior if both the mass function slope and the maximum mass were left as free parameters (all values $>20\ M_\odot$ were found to be consistent with the data if $\alpha \sim 4$). Therefore, we used two different approaches to fit our distributions. For one, we assumed the distribution followed a power-law function of the form $dN/dM \propto M^{-\alpha}$, with α left as a free parameter and with M_{max} fixed to 90 $M_\odot$. We also performed an MCMC run in which we fixed the functional form of the mass function to be a Salpeter IMF, $dN/dM \propto M^{-2.35}$, as one may expect to recover if all massive stars produce SNe. In these fits, M_{max} was constrained by the data. Weisz et al. (2013) explicitly notes that a meaningful limit on the maximum mass cannot be constrained by the data beyond simply returning the most massive star observed, so we emphasize that fit values for M_{max} in particular should be

Table 3
Progenitor Mass Results for M33 SNR Sample

SNR ID	M_{ZAMS} ($M_\odot$)	Progenitor Age (Myr)	MS Stars	Total Stars	Stellar Mass Formed (10^2 $M_\odot$)	Additional dA_V Applied (MATCH -dA_V Flag)
M33 SNR Progenitors						
20	$8.6^{+0.3}_{-0.3}$	38^{+2}_{-2}	1515	2816	44	0.2
30	$8.2^{+14.4}_{-0.7}$	42^{+8}_{-33}	1049	3014	91	0.6
34	24^{+4}_{-12}	$8.4^{+11.5}_{-1.3}$	1136	3024	150	0.8
37	10^{+1}_{-2}	27^{+17}_{-2}	368	1242	7	0
38	11^{+1}_{-4}	25^{+32}_{-2}	110	354	8	0
40	$7.7^{+3.8}_{-0.3}$	47^{+4}_{-24}	193	1008	51	0
41	$9.5^{+18.8}_{-2.5}$	31^{+25}_{-24}	1351	3317	120	0.6
43	16^{+3}_{-8}	14^{+31}_{-3}	188	1004	100	0
44	14^{+1}_{-7}	16^{+29}_{-2}	244	836	22	0
48	11^{+130}_{-1}	26^{+2}_{-24}	809	2805	72	0
49	$9^{+0.5}_{-0.6}$	35^{+5}_{-3}	1020	3081	78	0.3
50	19^{+1}_{-11}	11^{+39}_{-1}	125	628	74	0
57	$8.7^{+35.8}_{-1.2}$	37^{+13}_{-32}	824	4082	79	0.1
58	21^{+2}_{-12}	$9.8^{+25.7}_{-0.9}$	394	1170	160	0
59	12^{+1}_{-5}	20^{+25}_{-2}	905	3439	167	0.1
61	$15^{+\mathrm{INDEF}}_{-7}$	16^{+35}_{-14}	255	927	164	0
62	19^{+2}_{-7}	11^{+11}_{-1}	428	1470	114	0
63	$7.7^{+0.7}_{-0.2}$	47^{+3}_{-7}	353	1313	35	0
64	$7.7^{+0.2}_{-0.2}$	47^{+3}_{-3}	575	3559	35	0.1
66	$8.1^{+0.2}_{-0.2}$	42^{+2}_{-2}	352	1511	63	0
67	$7.8^{+1.1}_{-0.3}$	46^{+4}_{-11}	454	1938	66	0
69	$8.2^{+6.2}_{-0.3}$	41^{+3}_{-26}	1589	2090	161	0.3
71	11^{+12}_{-1}	26^{+2}_{-17}	1506	2639	133	0.1
74	$8.7^{+46.1}_{-0.3}$	37^{+3}_{-33}	580	1924	58	0
75	$9.9^{+7.2}_{-0.4}$	30^{+2}_{-17}	134	1063	118	0
76	$8.7^{+1.4}_{-0.4}$	37^{+3}_{-8}	705	2359	71	0
77	$8.7^{+\mathrm{INDEF}}_{-0.3}$	37^{+3}_{-34}	1145	2049	89	0.1
80	$8.6^{+0.3}_{-0.3}$	38^{+2}_{-2}	864	4120	84	0.2
81	14^{+6}_{-4}	16^{+12}_{-6}	1905	2372	243	0
83	16^{+101}_{-8}	13^{+22}_{-11}	1444	2221	391	0.2
84	$113^{+\mathrm{INDEF}}_{-103}$	$2.7^{+25.5}_{-1.9}$	68	315	10	0
91	10^{+1}_{-1}	28^{+3}_{-3}	1217	1816	29	0
134	$8.6^{+0.2}_{-0.3}$	37^{+2}_{-2}	349	874	14	0

considered illustrative. The precise values are not necessarily meaningful, whereas the fits for a free slope are more reliable.

The results from these fits are listed in Table 4. We do not attempt to evaluate which model description is a better fit to the data. There is evidence that the regions of progenitor masses over which SNe may explode may actually be quite complex (e.g., Sukhbold & Woosley 2014), making either parameterization of the mass distribution a likely oversimplification. However, the result of a paucity of massive progenitors is robust regardless of model selection. The use of the MCMC technique properly incorporates our measured uncertainties and rules out a Salpeter mass function for our progenitor sample.

We find that, independent of the sample that we fit, all distributions analyzed favor a model in which some fraction of the massive star population do not explode as SNe, whether it is parameterized as a very steep mass function or a Salpeter mass function with a cutoff. Furthermore, the M31 and M33 fit values indicate that both the slope and the maximum mass cutoff are consistent to within the uncertainties, suggesting that any metallicity or star formation intensity effects do not change the index by more than $\pm\sim1$. While this range in power-law indices is still large, the distributions are all still steeper than Salpeter regardless. A more precise comparison of the M31 and M33 distributions would naturally be interesting, but we are unable to make a more constraining statement than this given the current size of the data set and the uncertainties involved.

4.2. A Possible High Mass Cutoff for Producing SN

Both the individual M31 and M33 progenitor mass distributions, as well as the full progenitor mass distribution, are steeper than a Salpeter IMF with at least 95% confidence, regardless of the method used to fit the distribution. Thus, both the full sample and the individual M31 and M33 distributions display a paucity of massive stars compared to a simple model IMF. If we assume that a Salpeter distribution is a reasonable description of the massive star population, then this paucity suggests that some fraction of massive stars are not in our SNR progenitor sample. Recent theoretical and observational work has suggested that in certain mass ranges, massive stars may not undergo SN

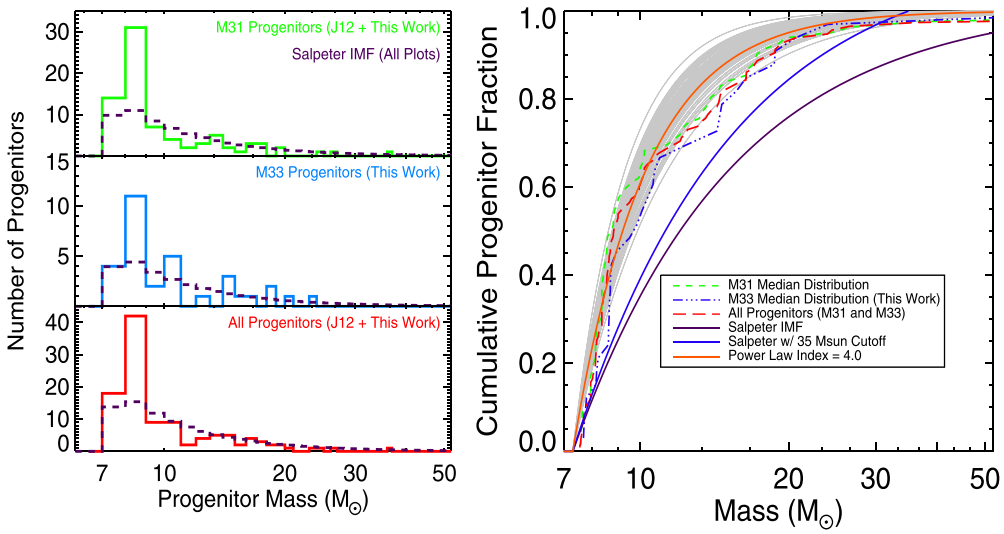

Figure 4. Left panels: histogram of median progenitor masses for all M31 progenitors (this work and J12), new M33 progenitors (this work), and all progenitors from both galaxies. Histograms which would be expected from a Salpeter ($\alpha = 2.35$) IMF are plotted in dashed yellow lines. The Salpeter histograms are normalized such that the total number of progenitors of the Salpeter distribution is the same as that observed in each sample. Right panel: cumulative distribution of median progenitor masses for same distributions. We also include a Salpeter IMF, a Salpeter IMF integrated only up to 35 $M_{\odot}$, and a power-law IMF with slope $\alpha = 4.0$. Note that all median mass distributions are steeper than a Salpeter IMF.

(A color version of this figure is available in the online journal.)

Table 4
MCMC Inferred Mass Distribution Parameters

Sample	Best Fit α[a]	Maximum Mass ($M_{\odot}$)[a]
Index α as Free Parameter, $M_{\rm max} = 90\,M_{\odot}$		
M31 Sample (J12 + This Work)	$\alpha = 4.4^{+0.4}_{-0.4}$	$M_{\rm max} = 90$
M33 Sample (This Work)	$\alpha = 3.8^{+0.5}_{-0.4}$	$M_{\rm max} = 90$
Full Sample (J12 + This Work)	$\alpha = 4.2^{+0.3}_{-0.3}$	$M_{\rm max} = 90$
Index Fixed to Salpeter ($\alpha = 2.35$), $M_{\rm max}$ as Free Parameter		
Full M31 Sample (J12 + This Work)	2.35	$M_{\rm max} = 38^{+15}_{-6}$
Full M33 Sample (This Work)	2.35	$M_{\rm max} = 41^{+45}_{-12}$
Full Distribution (J12 + This Work)	2.35	$M_{\rm max} = 35^{+5}_{-4}$

Note. [a] Quoted uncertainties come from 16th and 84th percentiles of the probability distributions.

explosions (e.g., Smartt et al. 2009; Horiuchi et al. 2011; Dessart et al. 2011; Sukhbold & Woosley 2014). Our observation is consistent with the interpretation that there are certain mass ranges in the massive star population in which stars fail to end their lives as CCSN.

4.3. Potential Effects From Biases in the SNR Sample

One important caveat is that the interpretation of an observed upper-mass CCSNe cutoff relies on sampling an unbiased population of massive stars, i.e., that our SNR catalogs are unbiased to any one type of progenitor star environment. Since we would expect higher-mass progenitors to be preferentially found in more-extincted regions, this may cause SNR from higher-mass progenitors to be systematically under-sampled in SNR catalogs. We have now expanded the sample to include SNR from M33, which is less inclined to our line of sight and lower metallicity (Bresolin 2011; Zurita & Bresolin 2012). Both of these qualities should reduce the amount of extinction, somewhat reducing these biases. However, we also note that a commonly used method for identifying SNRs is by their high [S II]/Hα flux ratios (e.g., Gordon et al. 1998). The youngest regions will have more photoionized H II, increasing the Hα flux and making SNR identification more difficult. We made some attempt to reduce this bias by incorporating SNR catalogs that use different methodology. In particular, the Long et al. (2010) M33 SNR catalog incorporates observations from radio to X-ray to catalog SNRs. In any case, given that SNRs do not stand out if they are located within a photo-ionized interstellar medium, we are currently unable to definitively distinguish between the possibility of SNRs from more-massive progenitors being more difficult to identify, and very high-mass stars not producing SNe.

In addition to difficulties in detection due to obscuration, any inherent differences in luminosity or lifetime of SNRs as a function of progenitor mass could also introduce some bias. These properties are dependent upon both the energy of the SN and the density of the medium into which the SNR expands. If one would appeal to this as an explanation for the lack of high mass progenitors, this would imply that SNR from higher mass stars have inherently lower luminosities and/or inherently shorter lifetimes. At present, we have no real ability to test either of these cases with our methodology. If there are significant differences in SNR frequencies or properties as a function of progenitor mass, then naturally we are no longer dealing with an unbiased sample of all exploded massive stars,

and our conclusions about the SNe progenitor mass distribution are weakened.

5. SUMMARY

In this work, we estimated progenitor masses of 33 SNRs in M33 and 29 SNRs in M31 using identical methodology to Jennings et al. (2012). After combining these with the 53 CCSNe progenitor mass estimates from J12, we constrain the progenitor distributions with a probabilistic technique which incorporates the uncertainties on the individual progenitor mass estimates. We find that the progenitor mass distributions of M31 and M33 both display a paucity of massive stars when compared to a Salpeter IMF. This suggests that some fraction of massive stars are not exploding as SNe, a similar finding to that seen in other theoretical and observational work (Smartt et al. 2009; Horiuchi et al. 2011; Dessart et al. 2011; Kochanek 2014). Our work represents an independent and complementary technique to these other methods. Now that the result has been expanded to M33, we have verified that this result holds across a range of galaxy inclination, metallicity, and morphology. However, we note that due to potential biases in the SNR catalogs, we cannot rule out the possibility that the SNR surveys have preferentially missed the SNRs of more massive SN progenitors.

In addition to this main result, we have also investigated other interesting properties of the progenitor mass distributions. Assuming a Salpeter IMF is the expected distribution if all massive stars produce SNe, we estimated the upper-mass cutoff necessary to be consistent with our data. The data from both galaxies are consistent with a maximum mass for core-collapse SNe of $\sim$35–45 $M_{\odot}$. We also compare the progenitor mass distributions of M33 and M31, finding them to be consistent with one another, albeit to within large uncertainties. At this stage, we believe we have examined all available archival *HST* data of sufficient depth to apply our stellar population analysis techniques in M31 and M33. We will be unable to offer a more precise comparison of the M31 and M33 SNR populations without additional observations of SNR in either galaxy.

Z.G.J. and B.F.W. are supported in part by AR-12834. B.F.W. is also supported in part by GO-12055. Z.G.J. is supported in part by a National Science Foundation Graduate Research Fellowship. This work is based on observations made with the NASA/ESA *Hubble Space Telescope*, obtained from the data archive at the Space Telescope Science Institute. Support for this work was provided by NASA through Hubble Fellowship grant 51273.01 awarded to K.M.G. by the Space Telescope Science Institute. STScI is operated by the Association of Universities for Research in Astronomy, Inc. under NASA contract NAS 5-26555. Support for D.R.W. is provided by NASA through Hubble Fellowship grant HST-HF-51331.01 awarded by the Space Telescope Science Institute.

REFERENCES

Badenes, C., Harris, J., Zaritsky, D., & Prieto, J. L. 2009, ApJ, 700, 727
Barker, M. K., Ferguson, A. M. N., Cole, A. A., et al. 2011, MNRAS, 410, 504
Barth, A. J., van Dyk, S. D., Filippenko, A. V., Leibundgut, B., & Richmond, M. W. 1996, AJ, 111, 2047
Bastian, N., & Goodwin, S. P. 2006, MNRAS, 369, L9
Blair, W. P., Kirshner, R. P., & Chevalier, R. A. 1982, ApJ, 254, 50
Braun, R., & Walterbos, R. A. M. 1993, A&AS, 98, 327
Bresolin, F. 2011, ApJ, 730, 129
Cappellaro, E., Evans, R., & Turatto, M. 1999, A&A, 351, 459
Crockett, R. M., Eldridge, J. J., Smartt, S. J., et al. 2008, MNRAS, 391, L5
Dalcanton, J. J., Williams, B. F., Lang, D., et al. 2012, ApJS, 200, 18
Dalcanton, J. J., Williams, B. F., Seth, A. C., et al. 2009, ApJS, 183, 67
Dessart, L., Hillier, D. J., Livne, E., et al. 2011, MNRAS, 414, 2985
Dolphin, A. E. 2000, PASP, 112, 1383
Dolphin, A. E. 2002, MNRAS, 332, 91
Efremov, Y. N. 1991, SvAL, 17, 173
Eldridge, J. J., Langer, N., & Tout, C. A. 2011, MNRAS, 414, 3501
Foreman-Mackey, D., Hogg, D. W., Lang, D., & Goodman, J. 2013, PASP, 125, 306
Fraser, M., Maund, J. R., Smartt, S. J., et al. 2012, ApJL, 759, L13
Fraser, M., Maund, J. R., Smartt, S. J., et al. 2014, MNRAS, 439, L56
Gal-Yam, A., & Leonard, D. C. 2009, Natur, 458, 865
Gal-Yam, A., Leonard, D. C., Fox, D. B., et al. 2007, ApJ, 656, 372
Girardi, L., Williams, B. F., Gilbert, K. M., et al. 2010, ApJ, 724, 1030
Gogarten, S. M., Dalcanton, J. J., Murphy, J. W., et al. 2009a, ApJ, 703, 300
Gogarten, S. M., Dalcanton, J. J., Williams, B. F., et al. 2009b, ApJ, 691, 115
Gordon, S. M., Kirshner, R. P., Long, K. S., et al. 1998, ApJS, 117, 89
Harris, J., & Zaritsky, D. 2009, AJ, 138, 1243
Hendry, M. A., Smartt, S. J., Crockett, R. M., et al. 2006, MNRAS, 369, 1303
Horiuchi, S., Beacom, J. F., & Dwek, E. 2009, PhRvD, 79, 083013
Horiuchi, S., Beacom, J. F., Kochanek, C. S., et al. 2011, ApJ, 738, 154
Jennings, Z. G., Williams, B. F., Murphy, J. W., et al. 2012, ApJ, 761, 26
Kochanek, C. S. 2014, ApJ, 785, 28
Kochanek, C. S., Beacom, J. F., Kistler, M. D., et al. 2008, ApJ, 684, 1336
Lada, C. J., & Lada, E. A. 2003, ARA&A, 41, 57
Li, W., Leaman, J., Chornock, R., et al. 2011, MNRAS, 412, 1441
Li, W., Van Dyk, S. D., Filippenko, A. V., & Cuillandre, J. 2005, PASP, 117, 121
Li, W., Van Dyk, S. D., Filippenko, A. V., et al. 2006, ApJ, 641, 1060
Li, W., Wang, X., Van Dyk, S. D., et al. 2007, ApJ, 661, 1013
Long, K. S., Blair, W. P., Winkler, P. F., et al. 2010, ApJS, 187, 495
Magnier, E. A., Prins, S., van Paradijs, J., et al. 1995, A&AS, 114, 215
Maíz-Apellániz, J., Bond, H. E., Siegel, M. H., et al. 2004, ApJL, 615, L113
Marigo, P., Girardi, L., Bressan, A., et al. 2008, A&A, 482, 883
Maund, J. R., Fraser, M., Ergon, M., et al. 2011, ApJL, 739, L37
Maund, J. R., Mattila, S., Ramirez-Ruiz, E., & Eldridge, J. J. 2014a, MNRAS, 438, 1577
Maund, J. R., Reilly, E., & Mattila, S. 2014b, MNRAS, 438, 938
Maund, J. R., Smartt, S. J., & Danziger, I. J. 2005, MNRAS, 364, L33
McConnachie, A. W., Irwin, M. J., Ferguson, A. M. N., et al. 2005, MNRAS, 356, 979
Murphy, J. W., Jennings, Z. G., Williams, B., Dalcanton, J. J., & Dolphin, A. E. 2011, ApJL, 742, L4
Panagia, N., Romaniello, M., Scuderi, S., & Kirshner, R. P. 2000, ApJ, 539, 197
Pietrinferni, A., Cassisi, S., Salaris, M., & Castelli, F. 2004, ApJ, 612, 168
Salpeter, E. E. 1955, ApJ, 121, 161
Schlegel, D. J., Finkbeiner, D. P., & Davis, M. 1998, ApJ, 500, 525
Smartt, S. J. 2009, ARA&A, 47, 63
Smartt, S. J., Eldridge, J. J., Crockett, R. M., & Maund, J. R. 2009, MNRAS, 395, 1409
Smartt, S. J., Maund, J. R., Hendry, M. A., et al. 2004, Sci, 303, 499
Smartt, S. J., Vreeswijk, P. M., Ramirez-Ruiz, E., et al. 2002, ApJL, 572, L147
Smith, N., Li, W., Filippenko, A. V., & Chornock, R. 2011a, MNRAS, 412, 1522
Smith, N., Li, W., Miller, A. A., et al. 2011b, ApJ, 732, 63
Sukhbold, T., & Woosley, S. E. 2014, ApJ, 783, 10
Thompson, T. A., Prieto, J. L., Stanek, K. Z., et al. 2009, ApJ, 705, 1364
Van Dyk, S. D., Cenko, S. B., Poznanski, D., et al. 2012a, ApJ, 756, 131
Van Dyk, S. D., Davidge, T. J., Elias-Rosa, N., et al. 2012b, AJ, 143, 19
Van Dyk, S. D., Li, W., Cenko, S. B., et al. 2011, ApJL, 741, L28
Van Dyk, S. D., Li, W., & Filippenko, A. V. 2003a, PASP, 115, 448
Van Dyk, S. D., Li, W., & Filippenko, A. V. 2003b, PASP, 115, 1289
Van Dyk, S. D., Peng, C. Y., Barth, A. J., & Filippenko, A. V. 1999, AJ, 118, 2331
Vinkó, J., Sárneczky, K., Balog, Z., et al. 2009, ApJ, 695, 619
Walborn, N. R., Phillips, M. M., Walker, A. R., & Elias, J. H. 1993, PASP, 105, 1240
Wang, X., Yang, Y., Zhang, T., et al. 2005, ApJL, 626, L89
Weisz, D. R., Fouesneau, M., Hogg, D. W., et al. 2013, ApJ, 762, 123
Williams, B. F., Schmitt, M. D., & Winkler, P. F. 1995, BAAS, 27, 883
Zurita, A., & Bresolin, F. 2012, MNRAS, 427, 1463